INL/CON-11-23761
PREPRINT

A Multidimensional and Multiphysics Approach to Nuclear Fuel Behavior Simulation

PHYSOR 2012

S. R. Novascone
R. L. Williamson
J. D. Hales
M. R. Tonks
D. R. Gaston
C. J. Permann
D. Andrs
R. C. Martineau

April 2012

The INL is a
U.S. Department of Energy
National Laboratory
operated by
Battelle Energy Alliance

PHYSOR 2012 Advances in Reactor Physics Linking Research, Industry, and Education
Knoxville, Tennessee, USA, April 15-20, 2012, on CD-ROM, American Nuclear Society, LaGrange Park, IL (2012)

A MULTIDIMENSIONAL AND MULTIPHYSICS APPROACH TO NUCLEAR FUEL BEHAVIOR SIMULATION

S. R. Novascone, R. L. Williamson, J. D. Hales, M. R. Tonks,
D. R. Gaston, C. J. Permann, D. Andrs, R. C. Martineau
Idaho National Laboratory
2525 N. Fremont Ave.
Idaho Falls, ID 83415 USA
stephen.novascone@inl.gov

ABSTRACT

Important aspects of fuel rod behavior are inherently multidimensional in addition to being complicated multiphysics problems. However, many current fuels modeling tools are strictly 2D axisymmetric or even 1.5D. This paper outlines the capabilities of a new fuel modeling tool able to analyze either 2D axisymmetric or fully 3D models. The need for multiphysics, multidimensional modeling is then demonstrated through a set of example problems. The first, a 10-pellet rodlet, demonstrates the viability of the solution method employed. This example highlights the effect of our smeared cracking model and also shows the multidimensional nature of discrete fuel pellet modeling. The second example relies on our multidimensional, multiphysics approach to analyze a missing pellet surface problem. As a final example, we show a 5-pellet rodlet simulation coupled to lower-length-scale simulations of bubble growth.

Key Words: nuclear fuel behavior, multiphysics, PCMI, multidimensional

1. INTRODUCTION

Nuclear fuel operates in an environment that induces complex multi-physics phenomena, occurring over distances ranging from inter-atomic spacing to meters, and times scales ranging from microseconds to years. This multi-physics behavior is often tightly coupled, a well known example being the thermomechanical behavior during final gap closure in light water reactor (LWR) fuel rods. Adding to this complexity, important aspects of fuel behavior are inherently three dimensional, examples including pellet-clad mechanical interaction (PCMI), fuel fracture, oxide formation and non-axisymmetric neutronics and cooling.

Current fuel rod simulation codes typically approximate this complex behavior using an axisymmetric, axially-stacked, one-dimensional radial representation (often referred to as 1.5D) [1][2][3] and, often, separate codes are used for steady and transient (or accident) conditions. Notable exceptions are the EPRI propriety code FALCON [4] which is 2D and can be applied to steady or transient operation, and the French code TOUTATIS [5] which is 3D, and typically used to investigate localized behavior. Current nuclear fuel simulation codes also rely heavily on correlational models derived from experimental data, limiting application to materials, geometries, and burnups where data are available. The need for improved modeling of PCMI [6] and, particularly, the importance of multidimensional capability for accurate fuel performance simulation [7] has been identified. A recent review article [8] clearly outlines the need for improved multi-physics, multi-dimensional, multi-scale capability for nuclear fuel simulation.

Since 2008 the Idaho National Laboratory (INL) has been developing next-generation capabilities to model nuclear fuel performance. Parallel efforts have included adapting the ABAQUS commercial thermomechanics code to model fuel behavior [9], and the development of a new multidimensional finite element fuels code called BISON. The BISON fuel behavior code, first described in [10], is the subject of this paper. Significant new capability has been included in BISON since that early paper, including application of the code to a variety of nuclear fuel problems.

We begin with a brief description of the computational framework used for BISON, and describe the governing equations used to solve 2D axisymmetric and 3D nuclear fuel performance problems. We then discuss results for a three applications which demonstrate the variety of problems that can be solved, as well as the need for multidimensional analysis. The first is an axisymmetric representation of a LWR fuel rodlet in which the fuel is modeled as discrete pellets rather than a smeared column. We next consider a 3D PCMI analysis of a section of a LWR fuel rod containing a missing pellet surface (MPS). The final application demonstrates BISON's ability to couple to lower-length scale models to account for material property variation with microstructural evolution.

2. BISON DESCRIPTION

2.1. Multi-physics Computational Framework

BISON is built using the INL Multiphysics Object-Oriented Simulation Environment, or MOOSE [11]. MOOSE is a parallel finite element-based framework for solving systems of coupled non-linear PDEs using the Jacobian-Free Newton Krylov (JFNK) method [12]. MOOSE supports the use of two and three-dimensional meshes and implicit time integration.

2.2. Governing Equations

The BISON governing relations currently consist of fully-coupled partial differential equations for energy and momentum conservation. The energy balance is given in terms of the heat conduction equation

$$\rho C_p \frac{\partial T}{\partial t} + \nabla \cdot \mathbf{q} - E_f \dot{F} = 0, \tag{1}$$

where T, ρ and C_p are the temperature, density and specific heat, respectively, E_f is the energy released in a single fission event, and $\dot{F}$ is the volumetric fission rate. $\dot{F}$ can be prescribed as a function of time and space, input from a separate neutronics calculation, or computed based on input rod average power and axial profile data. The heat flux is given as

$$\mathbf{q} = -k\nabla T, \tag{2}$$

where k denotes the thermal conductivity of the material.

Momentum conservation is prescribed assuming static equilibrium at each time increment using Cauchy's equation,

$$\nabla \cdot \boldsymbol{\sigma} + \rho \mathbf{f} = 0, \tag{3}$$

where $\boldsymbol{\sigma}$ is the Cauchy stress tensor and $\mathbf{f}$ is the body force per unit mass (e.g. gravity). The displacement vector $\mathbf{u}$, which is the primary solution variable, is connected to the stress field via the strain, through kinematic and constitutive relations.

2.3. Fuel Models

Focusing initially on UO_2 fuel, models have been included in BISON to describe temperature and burnup dependent thermal properties, solid and gaseous fission product swelling, densification, thermal and irradiation creep, pellet fracture via smeared cracking, and fission gas production, generation, and release.

The temperature-dependence of unirradiated material is defined using the equation suggested by Fink [13]. This relationship is then modified to account for the effects of irradiation, porosity and burnup using a series of multipliers, as outlined in detail by Lucuta et al. [14]. Empirical fits for the temperature dependent specific heat of UO_2 accompany the Fink-Lucuta model.

Swelling as a result of both solid and gaseous fission products is included using empirical relations from MATPRO [15]. Solid fission product swelling is expressed as a simple linear function of burnup:

$$\Delta\varepsilon_{sw-s} = 5.577 \times 10^{-5} \rho \Delta Bu \tag{4}$$

where $\Delta\varepsilon_{sw-s}$ is the volumetric solid swelling increment, ΔBu the burnup increment (fissions/atoms-U), and ρ is the density (kg/m^3). Swelling due to gaseous fission products is approximated by a semi-empirical model:

$$\Delta\varepsilon_{sw-g} = 1.96 \times 10^{-31} \rho \Delta Bu (2800 - T)^{11.73} e^{-0.0162(2800-T)} e^{-0.0178 \rho Bu} \tag{5}$$

where $\Delta\varepsilon_{sw-g}$ is the volumetric gas swelling increment, Bu and ΔBu are the burnup and burnup increment (fissions/atoms-U), respectively, ρ is the density (kg/m^3) and T is the temperature (K).

Fuel densification is computed using the ESCORE empirical model [4] given by:

$$\varepsilon_D = \Delta\rho_0 \left(e^{\left(\frac{Bu \ ln(0.01)}{C_D Bu_D} \right)} - 1 \right) \tag{6}$$

where ε_D is the densification strain, $\Delta\rho_0$ is the total densification that can occur (given as a fraction of theoretical density), Bu is the burnup, and Bu_D is the burnup at which densification is complete.

A model for combined secondary thermal creep and irradiation creep of UO_2 is available, with the creep rate modeled as a function of time, temperature, effective stress, density, grain size, fission rate, and oxygen-to-metal ratio (O/M). The constitutive relation is taken from the MATPRO FCREEP material model [16] and given as

$$\dot{\varepsilon} = \frac{A_1 + A_2 \dot{F}}{(A_3 + D) G^2} \sigma e^{\left(\frac{-Q_1}{RT} \right)} + \frac{A_4}{(A_6 + D)} \sigma^{4.5} e^{\left(\frac{-Q_2}{RT} \right)} + A_7 \dot{F} \sigma e^{\left(\frac{-Q_3}{RT} \right)} \tag{7}$$

where $\dot{\varepsilon}$ is the creep rate (1/s), σ is the effective (Mises) stress (Pa), T is the temperature (K), D is the fuel density (in percent of theoretical), G is the grain size (μm), $\dot{F}$ is the volumetric fission rate

(fissions/m^3-s), Q_i are the activation energies (J/mol), R is the universal gas constant, and A_{1-7} are material constants.

In ceramic fuel such as UO_2, a significant temperature gradient develops from the fuel center to the radial edge. This gradient appears early and is strong enough to induce cracking in the fuel due to the accompanying stress. The cracks reduce the stress in the fuel and increase the effective fuel volume (decrease the gap size). A smeared cracking model may be invoked to account for this cracking. The approach follows the one outlined in [17]. When the smeared cracking model is active, principal stresses are compared to a critical stress. If the material stress exceeds the critical stress, the material point is considered cracked in that direction, and the stress is reduced to zero. From that point on, the material point will have no strength unless the strain becomes compressive.

Fission gas release (FGR) is computed using the Forsberg-Massih two-stage analytical model [18]. The first stage of the Forsberg-Massih model computes fission gas diffusion to the grain boundary, based on an analytical solution to the diffusion equation in spherical coordinates. An effective diffusion coefficient is employed, which accounts for gas resolution and trapping within the fuel grain; the three-term coefficient developed by Turnbull [19] is used. In the second stage, time-dependent boundary conditions are used to determine grain boundary gas accumulation, resolution, saturation, and release parameters. Release from the grain boundaries is controlled using a grain boundary saturation criterion. Typical input parameters for UO_2 fuel, taken from Denis and Piotrkowski [20] were assumed.

2.4. Cladding Material Models

Focusing initially on Zircaloy as a clad material, models have been implemented for thermal and irradiation creep and irradiation growth.

Secondary thermal creep of zirconium alloys was recently thoroughly investigated by Hayes and Kassner [22] and found to be well-described by a traditional power-law creep formulation. The specific equation recommended there and implemented in BISON is

$$\dot{\varepsilon}_{ss} = A_0 \left(\frac{\sigma_m}{G} \right)^n e^{\left(\frac{-Q}{RT} \right)} \tag{8}$$

where $\dot{\varepsilon}_{ss}$ is the effective thermal creep rate (1/s), σ_m is the effective (Mises) stress (Pa), Q is the activation energy (J/mol), R is the universal gas constant (J/mol-K), T is the temperature (K), G is the shear modulus (Pa), and A_0 and n are material constants. Parameters for this model were taken from [22] and [23]. Note that a model for primary creep of zirconium alloys has not yet been implemented in BISON.

Irradiation-induced creep of cladding materials is based on an empirical model developed by Hoppe [24] that relates the creep rate to the current fast neutron flux and stress. The specific relation implemented is:

$$\dot{\varepsilon}_{ir} = C_0 \Phi^{C_1} {\sigma_m}^{C_2} \tag{9}$$

where $\dot{\varepsilon}_{ir}$ is the effective irradiation creep rate (1/s), Φ is the fast neutron flux (n/m^2-s), σ_m is the effective (Mises) stress (MPa), and C_0, C_1, and C_2 are material constants. Note that the original

Hoppe formulation is given in terms of circumferential stress, whereas the relation implemented in BISON assumes an effective (Mises) stress.

Cladding elongation as a result of radiation-induced growth is included using the ESCORE empirical model [4] given by:

$$\varepsilon_g = A_g(\Phi t)^{n_g} \tag{10}$$

where ε_g is the irradiation growth strain, Φt is the fast neutron fluence (n/cm^2), and A_g and n_g are material constants that depend on the cladding metallurgical state. From [4], typical values for stress-relieved Zr-2 and Zr-4 are $A_g = 3 \times 10^{-20}$ and $n_g = 0.794$.

2.5. Gap/Plenum Models

We now outline models for gap heat transfer, mechanical contact, and gap/plenum pressure.

Gap heat transfer is modeled using the relation,

$$h_{gap} = h_g + h_s + h_r \tag{11}$$

where h_{gap} is the total conductance across the gap, h_g is the gas conductance, h_s is the increased conductance due to solid-solid contact, and h_r is the conductance due to radiant heat transfer. The increased conductance due to solid-solid contact, h_s, as described by Olander [25], is still to be implemented.

The gas conductance h_g is described using the form proposed by Ross and Stoute [26]:

$$h_g = \frac{k_g(T_g)}{d_g + C_r(r_1 + r_2) + g_1 + g_2} \tag{12}$$

where k_g is the conductivity of the gas in the gap, d_g is the gap width, C_r is a roughness coefficient with r_1 and r_2 the roughnesses of the two surfaces, and g_1 and g_2 are jump distances at the two surfaces. The conductivity of the gas mixture (k_g) is computed using the mixture rule from MATPRO [16], which permits mixtures of several gases.

The conductance due to radiant heat transfer, h_r, is computed using a diffusion approximation based on the Stefan-Boltzman law. Because fuel/pellet gaps are typically very narrow in comparison to the pellet radius, the required emissivity function is approximated using the formulation for infinite parallel plates.

Mechanical contact between fuel pellets and the inside surface of the cladding is based on three requirements:

$$g \leq 0, \quad t_N \geq 0, \quad t_N g = 0. \tag{13}$$

That is, the penetration distance g of one body into another must not be positive; the contact force t_N opposing penetration must be positive in the normal direction; and either the penetration distance or the contact force must be zero at all times.

In BISON, these contact constraints are enforced through the use of node/face constraints. Specifically, the nodes of the fuel pellets are prevented from penetrating the faces of the cladding.

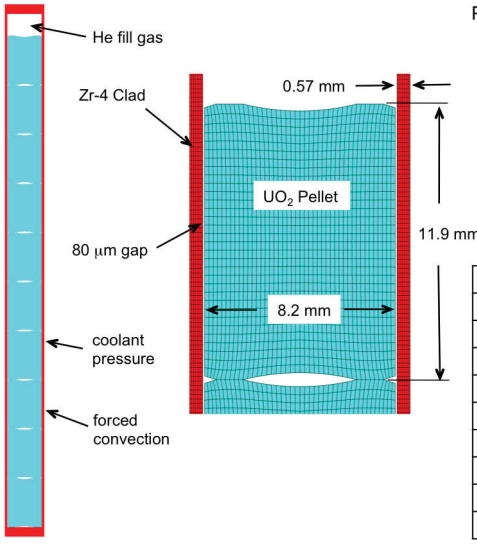

Linear average power	200 W/cm
Fast neutron flux	9.5×10^{17} n/m^{2}s
Coolant pressure	15.5 MPa
Coolant temperature (uniform)	530 K
Coolant convection coefficient	7500 W/m^{2}K
Rod fill gas	helium
Fill gas initial pressure	2.0 MPa
Initial fuel density	95% theoretical
Fuel densification	1% theoretical
Burnup at full densification	5 MWd/kgU

Figure 1. Axisymmetric problem geometry, power history, and operating conditions.

This is accomplished in a manner similar to that detailed by Heinstein and Laursen [27]. To date, BISON supports tied and frictionless contact with frictional contact still to be implemented.

The pressure in the gap and plenum is computed based on the ideal gas law,

$$P = \frac{nRT}{V} \tag{14}$$

where P is the gap/plenum pressure, n is the moles of gas, R is the ideal gas constant, T is the temperature, and V is the volume of the cavity. The moles of gas, the temperature, and the cavity volume in this equation are free to change with time.

3. Demonstration Problems

In this section we show results from three BISON simulations. These problems were selected to showcase representative, though not comprehensive, examples of nuclear fuel simulation. The results shown here are from a 2D LWR fuel rod, a 3D LWR fuel rod with a missing pellet surface, and an example of a lower-length-scale simulation that is coupled to a continuum-scale simulation.

3.1. Axisymmetric Discrete-pellet Fuel Rod

The various modeling capabilities of BISON are demonstrated using a 2D axisymmetric analysis of a simplified fuel rodlet. The assumed geometry and power history are shown in Figure 1. The problem includes ten individual UO_2 pellets, Zr-4 cladding, an initial 80 μm pellet-clad gap, and an open region to simulate the upper plenum. The plenum volume was set assuming a plenum to fuel length ratio of 0.045, typical for PWR fuel [28, p. 282]. A uniform convective boundary

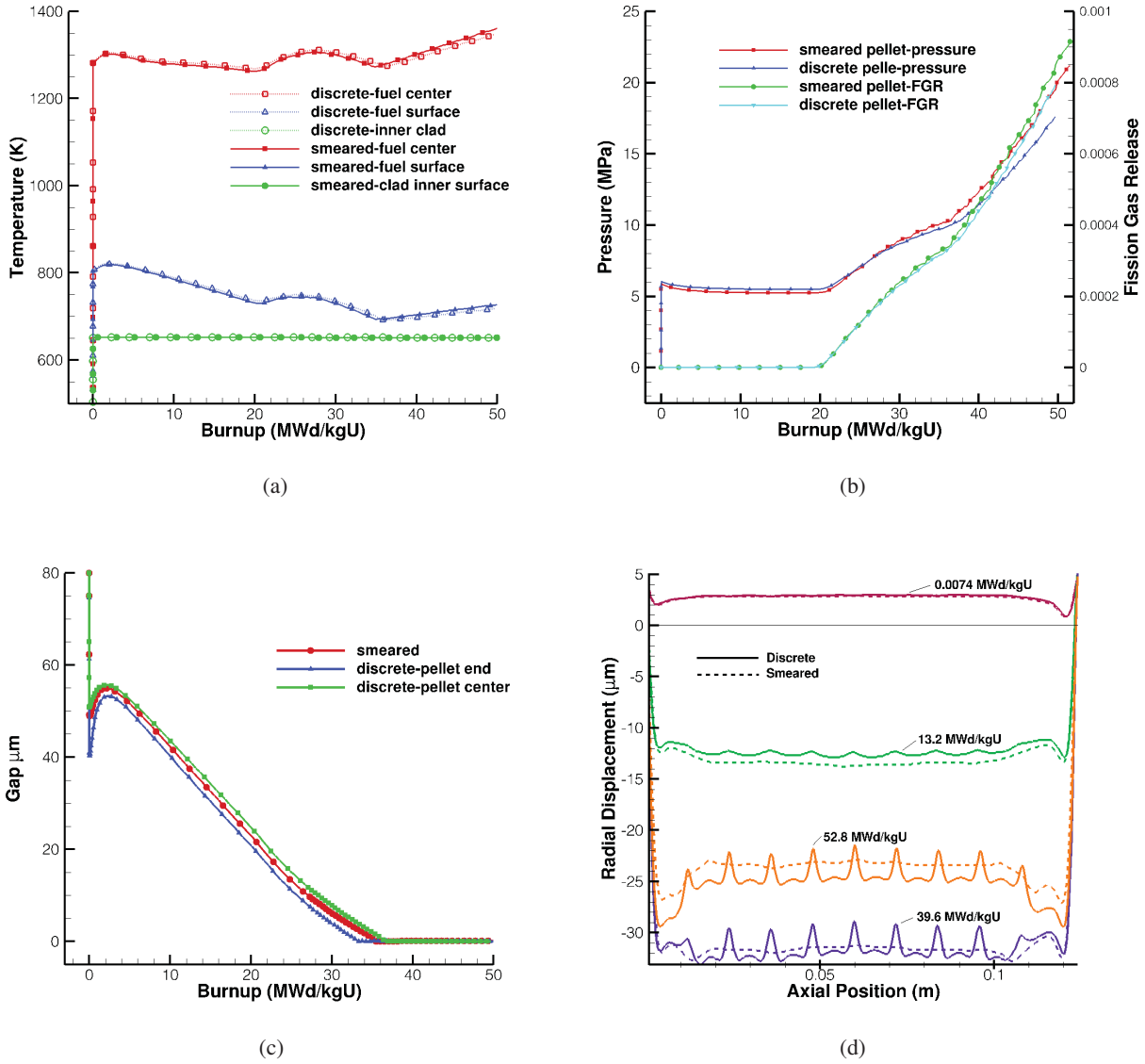

Figure 2. Results from the 2D axisymmetric ten pellet rodlet simulation for both smeared and discrete pellets, where (a) shows temperature plots at three locations in the fuel and (b) shows the pressure and fission gas release. The gap size is found in (c), while the radial displacement of cladding vs axial position is shown in (d). Note the bambooing effect due to discrete pellets.

condition at the clad outer wall simulates heat transfer to the flowing coolant. Operating conditions typical of a PWR reactor were used, as given in Figure 1. Although not realistic for the short rod length considered, a constant axial power profile was applied to the fuel to demsonstrate this capability.

UO_2 properties were taken from [25, Chap. 10 and 16], while temperature dependent thermal and elastic properties for Zr-4 were taken from MATPRO [15]. The contact surface between the fuel

and clad is assumed frictionless. For this demonstration problem, mesh resolution studies were not performed. Note that results in which the 10 discrete pellets are simulated with a single smeared pellet are shown for comparison.

Results for temperature at the fuel centerline, fuel radial surface, and inner clad surface for the smeared and discrete-pellet simulations are shown in Figure 2(a). Following the initial power ramp, the fuel centerline temperature first increases slightly due to an increase in the fuel-clad gap as a result of fuel densification. After densification, fuel swelling and clad creep combine to reduce the gap size, resulting in a decrease in fuel temperature.

Fission gas release begins at a burnup of 20 MWd/kgU, and plots of fission gas release and the corresponding increase in plenum pressure are shown in Figure 2(b). As gas is released to the gap a corresponding increase in fuel temperature occurs, evident in Figure 2(a), due to a reduction in gap gas thermal conductivity as the fission gas mixes with the helium fill gas. This temperature increase is gradually reversed by continual gap closure, until the gap is fully closed at approximately 36 MWd/kgU. Fuel temperatures increase from this point on, due to decreasing fuel thermal conductivity with burnup.

The predicted gap width versus burnup, at both a pellet end and axial centerline, is shown in Figure 2(c). Results from both the discrete and smeared-pellet calculations are shown for comparison. Note that the gap closes earlier at the end of the pellet, which is evidence of the so-called “bambooing” effect that has been observed in LWR fuel rods. This effect can be clearly seen in Figure 2(d), which compares the cladding radial displacement for the smeared and discrete pellet cases, at four burnup levels. The multidimensional bambooing effect of the discrete pellets becomes obvious following pellet-clad contact.

3.2. Missing Pellet Surface

Instances of cladding failure due to PCMI occur for a variety of reasons. One example occurs in high energy reactor cores when there is a fuel pellet geometric imprefection known as missing pellet surface (MPS) [29]. The presence of the MPS increases the gap between the fuel and clad, resulting in a corresponding increase in the fuel temperature. This increase in temperature also increases fuel swelling due to both thermal expansion and gaseous fission product swelling. This is similar to a power increase but with the added complication of localizing a large hoop stress in the section of clad directly across from the MPS (a 3D effect) that can lead to a through-thickness crack in the clad. This failure scenario has been studied previously [29], [30] using a combination of 2D axisymmetric and plane-strain analyses. We present a 3D simulation of a MPS problem using BISON.

The assumed geometry is shown in Figure 3(a), and includes a MPS pellet placed midway between four intact pellets. A magnified view of the mesh near the MPS is included in Figure 3(a). This simulation was run from a fresh fuel state with a typical power history, followed by a late-life power ramp.

Temperatures in the fuel and clad are shown in Figure 3(b), and clearly demonstrate the localized increase in fuel temperature due to the MPS. The temperature and deformation of the cladding is also significantly impacted by the MPS, as shown in Figure 3(c) (where the displacements are

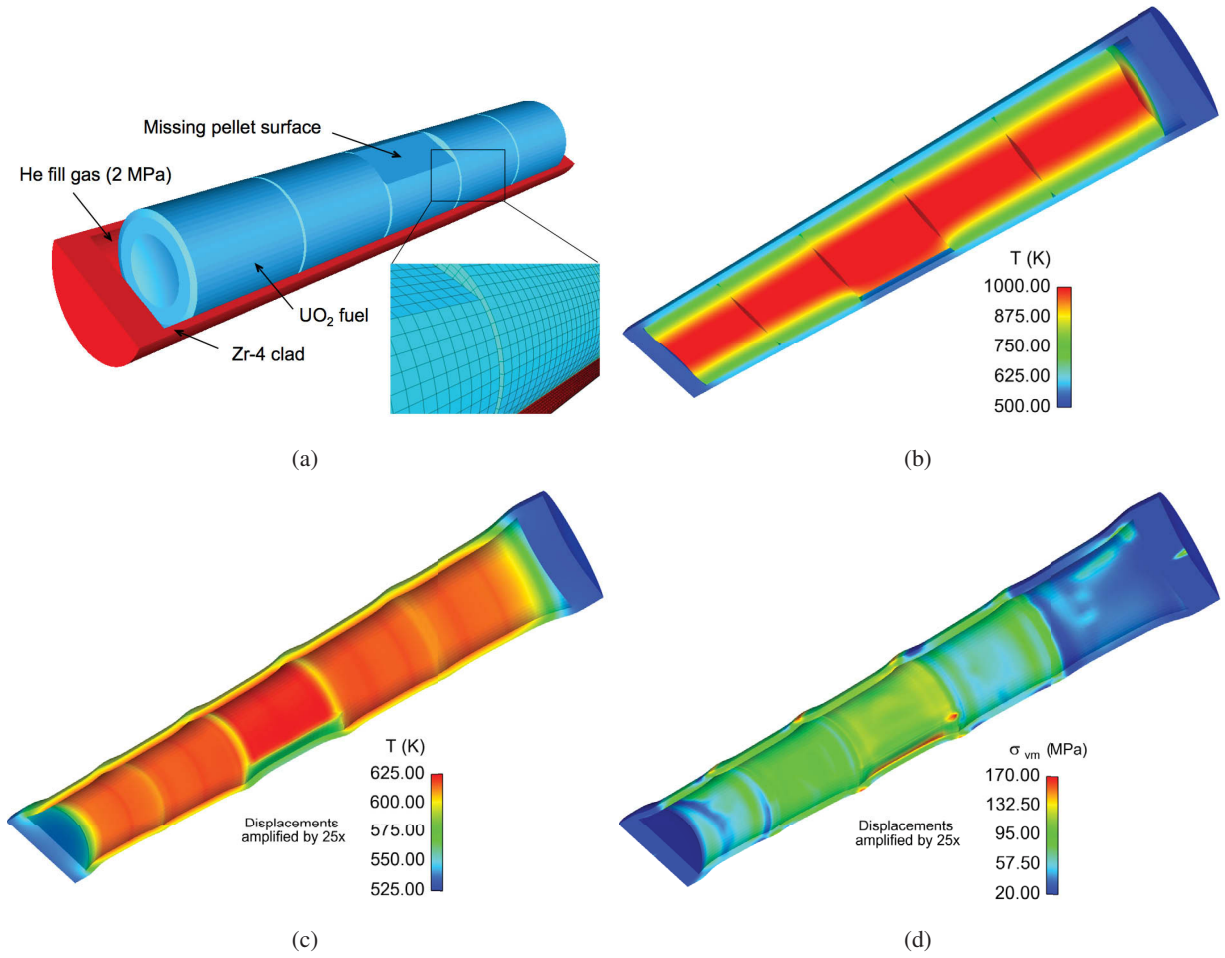

Figure 3. Results from the 3D missing pellet surface simulation, where (a) illustrates the geometry and materials from the simulation and the computational mesh near the MPS is shown in the inset. The temperature results in the fuel and clad are shown in (b), the temperature in the clad is shown in (c) and the effective stress (von Mises) in the clad is shown in (d). The displacements are magnified 25× in (c) and (d).

magnified by 25 times). These effects lead to higher stress in the clad (Fig. 3(d)), possibly resulting in clad cracking and ultimately failure.

3.3. Coupling to Lower Length Scale

As discussed in the introduction, radiation damage causes changes in the macroscale material response. These effects are traditionally considered using empirical models from experimental data. While these models can accurately interpolate between experimental values, they cannot extrapolate to different conditions or consider changes in the material. However, using modeling and simulation tools at various scales, mechanistic models can be developed to replace the empirical correlations. Multiscale models can be hierarchical, where the models at the various scales are run separately to develop constitutive equations, or concurrent, where the models are

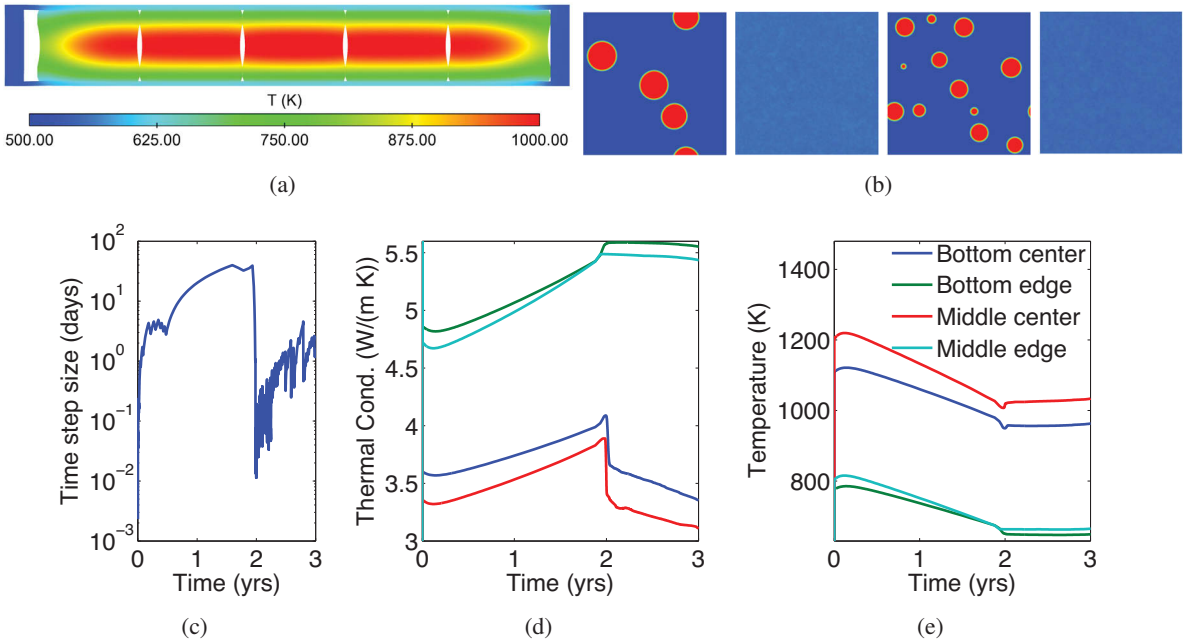

Figure 4. Multiscale simulation results, where (a) shows the final geometry of the rodlet and (b) shows the final microstructure at the center of the middle pellet (left), outer edge of the middle pellet (left center), center of the bottom pellet (right center) and the edge of the bottom pellet (right). In addition, the behavior of the time step during the simulation is shown in (c), and the thermal conductivity (d) and temperature (e) are shown vs time at the four locations.

run simultaneously and information is passed between the scales. Hierarchical coupling is by far the most efficient, but can miss important interactions between the scales. Thus, concurrent coupling is necessary to investigate the importance of such interactions. BISON has been used for both forms of coupling [32], though we only highlight concurrent coupling here, since it represents a unique capability of BISON.

We couple a BISON simulation to phase field simulations using the MOOSE-based code MARMOT [33] for a simple, proof-of-concept simualtion. The BISON simulation is a 2D axisymmetric simulation of a five pellet rodlet similar to the ten pellet rodlet discussed above. The materials models are identical to those used above except for the thermal conductivity, which is taken from the mesoscale simulations. Four simulations of bubble nucleation and growth in a micron square of UO_2 are solved using the bubble growth model from [33] in which only the vacancy concentration is considered. Note that due to the simplicity of this model, bubble nucleation occurs much later than the true physical behavior. A random source term accounts for the vacancies generated due to radiation and is a function of the neutron flux. A steady-state heat conduction calculation is coupled to the phase field model to determine changes in the bulk thermal conductivity.

The BISON simulation is loosely coupled to the four MARMOT simulations, with the BISON calculation occurring first at each time step. The mesoscale simulations are assigned to the center

of the middle pellet, the outer edge of the middle pellet, the center of the bottom pellet and the edge of the bottom pellet, and the corresponding temperature and neutron flux are passed down to define the boundary conditions of the corresponding phase field simulations. The four microstructures are evolved and the thermal conductivity is calculated at the four positions. These values are then linearly interpolated throughout the five pellets, with the thermal conductivity of the bottom pellet mirrored to the top pellet. The interpolated values are used in the BISON simulation at the next time step. All the simulations take the same time step, following the smallest required time step of the five simulations.

The temperature profile in the rodlet after three years is shown in Figure 4(a) and the final microstructure at the four locations within the rodlet are shown in Figure 4(b). The bubbles are most developed at the center of the middle pellet, due to the high temperature and neutron flux. At the outer edge of both pellets, the temperature is too low for significant vacancy diffusion and clustering. Thus, no bubbles form. Before the formation of the bubbles, the time step was quite high ($\sim$ 50 days) as shown in Figure 4(c). However, once bubbles begin to nucleate, the time step dropped three orders of magnitude to $\sim$ 0.01 days.

The thermal conductivity decreases at the center of the middle pellet after bubble nucleation (see Figure 4(d)). Due to this drop, the temperature rises throughout the rodlet (Figure 4(e)), accelerating the nucleation in the center of the bottom pellet. Thus, the interaction between the scales plays in important role in the bubble nucleation and thus the thermal conductivity behavior.

4. CONCLUSIONS

We have reviewed the capabilities of a new fuel performance code, BISON, that is capable of multidimensional, multiphysics analysis of nuclear fuel behavior. We have demonstrated the effectiveness of BISON on a set of demonstration problems. These have shown the need for multidimensional approaches for defect analysis, but multidimensional approaches are useful for many types of analyses.

Future work in BISON will include expanding its nuclear fuel behavior capabilities in order to be a full-featured application. Work is underway to couple BISON to more meso-scale models as well as reactor-level models for neutronics. BISON validation studies have begun and initial comparisons to integral fuel rod tests show good agreement; these studies will be reported elsewhere in the near future.

ACKNOWLEDGEMENTS

The submitted manuscript has been authored by a contractor of the U.S. Government under Contract DE-AC07-05ID14517. Accordingly, the U.S. Government retains a non-exclusive, royalty-free license to publish or reproduce the published form of this contribution, or allow others to do so, for U.S. Government purposes.

REFERENCES

[1] G. A. Berna, C. E. Beyer, K. L. Davis, and D. D. Lanning. “FRAPCON–3: A Computer Code for the Calculation of Steady-State, Thermal-Mechanical Behavior of Oxide Fuel Rods

for High Burnup." Technical Report NUREG/CR-6534 Vol. 2, PNNL–11513 (1997).

[2] K. Lassmann, A. Schubert, and J. van de Laar. "TRANSURANUS Handbook." Technical Report Document Number Version 1 Modification 1 Year 2003 (V1M1J2003) (2003).

[3] W. J. Kilgour, J. A. Turnbull, R. J. White, A. J. Bull, P. A. Jackson, and I. D. Palmer. "Capabilities and validation of the ENIGMA fuel performance code." In *Proceedings of the ENS Meeting on LWR Fuel Performance*. Avignon, France (1992).

[4] Y. Rashid, R. Dunham, and R. Montgomery. "Fuel Analysis and Licensing Code: FALCON MOD01." Technical Report EPRI 1011308, Electric Power Research Institute (2004).

[5] F. Bentejac and N. Hourdequin. "TOUTATIS: An application of the CAST3M finite element code for PCI three-dimensional modeling." In *Proceedings of Pellet-clad Interaction in Water Reactor Fuels*, pp. 495–506. Aix-en-Provence, France (2004).

[6] J. Killeen, E. Sartori, and T. Tverberg. "FUMEX-III: A new IAEA coordinated research project on fuel modeling at extended burnup, Paper 2176." In *Proceedings of Top Fuel 2009*. Paris, France (2009).

[7] In *Proceedings of Pellet-clad Interaction in Water Reactor Fuels*, p. 23. Aix-en-Provence, France (2004).

[8] J. Rashid, S. Yagnik, and R. Montgomery. "Light water reactor fuel performance modeling and multi-dimensional simulation." *JOM Journal of the Minerals, Metals and Materials Society*, **volume 63**, pp. 81–88 (2011). URL http://dx.doi.org/10.1007/s11837-011-0144-9.

[9] R. L. Williamson. "Enhancing the ABAQUS thermomechanics code to simulate multipellet steady and transient LWR fuel rod behavior." *Journal of Nuclear Materials*, **volume 415**, p. 74 (2011).

[10] C. Newman, G. Hansen, and D. Gaston. "Three Dimensional Coupled Simulation of Thermomechanics, Heat, and Oxygen Diffusion in UO_2 Nuclear Fuel Rods." *Journal of Nuclear Materials*, **volume 392**, pp. 6–15 (2009).

[11] D. Gaston, C. Newman, G. Hansen, and D. Lebrun-Grandié. "MOOSE: A parallel computational framework for coupled systems of nonlinear equations." *Nucl Eng Design*, **volume 239**, pp. 1768–1778 (2009).

[12] D. A. Knoll and D. E. Keyes. "Jacobian-Free Newton-Krylov Methods: a Survey of Approaches and Applications." *J Comput Phys*, **volume 193**(2), pp. 357–397 (2004).

[13] J. K. Fink. "Thermophysical properties of uranium dioxide." *J Nucl Materials*, **volume 279**(1), pp. 1–18 (2000).

[14] P. G. Lucuta, H. J. Matzke, and I. J. Hastings. "A pragmatic approach to modelling thermal conductivity of irradiated UO_2 fuel: review and recommendations." *Journal of Nuclear Materials*, **volume 232**, pp. 166–180 (1996).

[15] C. M. Allison, G. A. Berna, R. Chambers, E. W. Coryell, K. L. Davis, D. L. Hagrman, D. T. Hagrman, N. L. Hampton, J. K. Hohorst, R. E. Mason, M. L. McComas, K. A. McNeil, R. L. Miller, C. S. Olsen, G. A. Reymann, and L. J. Siefken. "SCDAP/RELAP5/MOD3.1 Code Manual, Volume IV: MATPRO–A Library of Materials Properties for Light-Water-Reactor Accident Analysis." Technical Report NUREG/CR-6150, EGG-2720, Idaho National Engineering Laboratory (1993).

[16] C. M. Allison and et al. "SCDAP/RELAP5/MOD3.1 Code Manual Volume IV: MATPRO." Technical Report NUREG/CR-6150, Idaho National Laboratory (1993).

[17] Y. R. Rashid. "Mathematical modeling and analysis of fuel rods." *Nucl Engrg Design*, **volume 29**, pp. 22–32 (1974).

[18] K. Forsberg and A. R. Massih. "Diffusion theory of fission gas migration in irradiated nuclear fuel UO_2." *Journal of Nuclear Materials*, **volume 135**(2-3), pp. 140–148 (1985).

[19] J. A. Turnbull, R. White, and C. Wise. "The diffusion coefficient for fission gas atoms in UO_2." Technical Report IAEA-TC-659/3.5 (1987).

[20] A. Denis and R. Piotrkowski. "Simulation of isothermal fission gas release." *Journal of Nuclear Materials*, **volume 229**, pp. 149–154 (1996).

[21] C. Vitanza, E. Kolstad, and U. Graziani. "Fission Gas Release from UO2 Pellet Fuel at High Burnup." In *Proceedings of the American Nuclear Society Meeting on Light Water Reactor Fuel Performance*, p. 361. Portland, Oregon (1979).

[22] T. A. Hayes and M. Kassner. "Creep of Zirconium and Zirconium Alloys." *Metallurgical and Materials Transactions A*, **volume 37A**, pp. 2389–2396 (2006).

[23] J. Moon, P. Cantonwine, K. Anderson, S. Karthikeyan, and M. Mills. "Characterization and modeling of creep mechanisms in Zircaloy-4." *Journal of Nuclear Materials*, **volume 353**(3), pp. 177 – 189 (2006). URL http://www.sciencedirect.com/science/article/pii/S0022311506001759.

[24] N. E. Hoppe. "Engineering model for zircaloy creep and growth." In *Proceedings of the ANS-ENS International Topical Meeting on LWR Fuel Performance*, pp. 157–172. Avignon, France (1991).

[25] D. R. Olander. *Fundamental aspects of nuclear reactor fuel elements*. Technical Information Center, Energy Research and Development Administration (1976).

[26] A. M. Ross and R. L. Stoute. "Heat transfer coefficient between UO_2 and Zircaloy-2." Technical Report AECL-1552, Atomic Energy of Canada Limited (1962).

[27] M. Heinstein and T. Laursen. "An algorithm for the matrix-free solution of quasistatic frictional contact problems." *Int J Numer Meth Engrg*, **volume 44**, pp. 1205–1226 (1999).

[28] H. Bailly, D. Ménessier, and C. Prunier, editors. *The Nuclear Fuel of Pressurized Water Reactors and Fast Neutron Reactors*. Lavoisier Publishing, Paris, France (1999).

[29] Y. Aleshin, C. Beard, G. Mangham, D. Mitchell, E. Malek, and M. Young. "The effect of pellet and local power variations on PCI margin." In *Proceedings of Top Fuel, 2010*. Orlando, FL, USA (2010).

[30] F. Groeschel, G. Bart, R. Montgomery, and S. K. Yagnik. "Failure root cause of a pci suspect liner fuel rod." In *IAEA Techincal Meeting on Fuel Failure in Water Reactors: Causes and Mitigation*. Bratislave, Slovakia (2002).

[31] P. C. Millett and M. Tonks. "Meso-scale modeling of the influence of intergranular gas bubbles on effective thermal conductivity." *Journal of Nuclear Materials*, **volume 412**(3), pp. 281 – 286 (2011). URL http://www.sciencedirect.com/science/article/pii/S0022311511002376.

[32] M. R. Tonks, G. Hansen, D. Gaston, C. Permann, P. Millett, and D. Wolf. "Fully-coupled Engineering and Mesoscale Simulations of Thermal Conductivity in UO_2 Fuel Using an Implicit Multiscale Approach." *Journal of Physics: Conference Series*, **volume 180**(1), p. 012078 (2009).

[33] M. Tonks, D. Gaston, P. Millett, D. Andrs, and P. Talbot. "An object-oriented finite element framework for multiphysics phase field simulations." *Comp Mat Sci*, **volume 51**(1), pp. 20–29 (2012).